Detection of Lines and Boundaries in Speckle Images—Application to Medical Ultrasound

Richard N. Czerwinski, *Member, IEEE*, Douglas L. Jones, *Senior Member, IEEE*, and William D. O'Brien, Jr.,* *Fellow, IEEE*

***Abstract*— This paper describes an approach to boundary detection in ultrasound speckle based on an image enhancement technique. The enhancement algorithm works by filtering the image with "sticks," short line segments which are varied in orientation to achieve the maximum projected value at each point. The statistical properties of this approach have been described in an earlier paper; in this work we present three significant extensions to improve the performance of the basic method. First, we investigate the effect of varying the size and shape of the sticks. We show that these variations affect the performance of the algorithm in very fundamental ways, for example by making it more or less sensitive to thinner or more tightly curving boundaries. Second, we present a means of improving the performance of this technique by estimating the distribution function of the orientation of the line passing through each point. Finally, we show that images can be "stained" for easier visual interpretation by applying to each pixel a false color whose hue is related to the orientation of the most prominent line segment at that point. Examples are given to illustrate the performance of the different settings on a single image.**

***Index Terms*— Boundary detection, image enhancement, speckle, ultrasound.**

I. Introduction

MEDICAL ultrasound is a pulse-echo imaging modality capable of quickly producing high-resolution images of soft tissue structures. Because commercial ultrasound systems are used predominantly in real-time diagnostic situations, the images they produce are generally optimized for visual interpretation of qualitative information about the tissue being scanned. Often, however, *quantitative* information about a scan, such as the size of a macroscopic tissue structure, is also of significant interest, as is the case in fetal maturity estimation. In these cases, the speckle texture which provides diagnostic information to the clinician may corrupt machine estimates of the positions of the boundaries.

Manuscript received March 12, 1998; revised October 6, 1998. This work was performed at the Department of Electrical and Computer Engineering at the University of Illinois at Urbana-Champaign, and was supported in part by the National Live Stock and Meat Board, by the United States Department of Agriculture, and by the National Cancer Institute, DHHS under Grant PHS Grant 5 T32 CA 09067. The Associate Editor responsible for coordinating the review of this paper and recommending its publication was C. R. Meyer. *Asterisk indicates corresponding author.*

R. N. Czerwinski is with the Lincoln Laboratory, Massachusetts Institute of Technology, Lexington, MA USA.

D. L. Jones is with the Department of Electrical and Computer Engineering, University of Illinois at Urbana-Champaign, Urbana, IL 61801 USA.

*W. D. O'Brien, Jr. is with the Department of Electrical and Computer Engineering, University of Illinois at Urbana-Champaign, Urbana, IL 61801 USA (e-mail: wdo@uiuc.edu).

Publisher Item Identifier S 0278-0062(99)02776-7.

The boundaries of interest in an ultrasound scan correspond to discontinuities between tissue layers, which are large on the scales of both the wavelength of interrogation and the scan line spacing. In the two-dimensional (2-D) scan plane, these three-dimensional (3-D) surfaces take on the appearance of bright streaks against a darker, less densely reflecting background. Features with this appearance are unlikely to occur randomly in speckle noise; speckle's correlation structure is more likely to give rise to bright spots of characteristic size [1]. Conventional edge detection procedures, e.g., Canny, Roberts, or Sobel operators [2], [3] and related techniques such as [4], are ill-suited to detect the boundaries because they are not well modeled as step discontinuities in image intensity. In contrast, we have had success with an approach designed to respond preferentially to *line processes* [5], [6]. This approach results in an operator that is sensitive even to thin edges, while still providing for speckle reduction.

To formalize this idea, we have approached the problem of boundary detection with the techniques of statistical decision theory. This has led to a number of detection rules motivated by a statistical model for the targets and noise. In [7], we derived optimal boundary detection techniques, and tested them in simulated speckle to establish performance bounds for other detectors. We compared several suboptimal detectors of varying complexity and power with the bounds, and showed that a simple suboptimal detector based on the generalized likelihood ratio test (GLRT) is extremely robust in the face of an uncertain or inexactly modeled statistical environment. Furthermore, we were able to quantify the performance lost in using this detector, and identify circumstances in which that loss was negligible [7]. The present work studies that detector in more detail, focusing in part on a number of different parameters which can be changed to alter its properties, such as the length and thickness of the templates used to model the boundaries.

This paper also addresses a weakness of the technique in [7], the assumption that all orientation sticks are equally likely at each point. In practice this is not the case, since B-mode ultrasound is most sensitive to the surfaces of structures normal to the beam. To improve upon the performance of the basic technique, the image itself can be used to estimate a distribution on the angle of the lines at each point in the image. This prior information can help to reject unlikely hypotheses.

Finally, we discuss the use of false color as a visualization tool to indicate the direction of the most prominent linear image feature at each point. The color can be applied to either the original or a processed image, and represents a

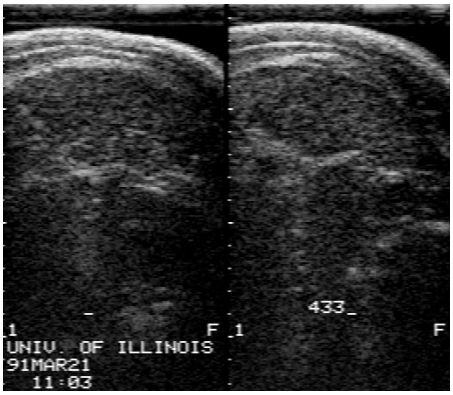

Fig. 1. Original image, showing the longissimus muscle of a live pig.

way of displaying additional information on an image without changing the image gray scale itself. This is an important issue in medical ultrasound, where sonographers are skilled in interpreting unprocessed gray level images.

These issues are somewhat apart from simple detector power. In [7], the detection scenario was carefully controlled so that the target and noise statistics were known; here the various tradeoffs will be quantified by showing the effect of the different settings on the processing of a single real image. This test image is given in Fig. 1, a scan of the longissimus muscle of a live pig, imaged with a PIE medical ultrasound scanning system and a Targa 16 Image Processing card. This image shows the muscle and several subcutaneous fat layers whose relative thicknesses are of interest. Each half of this image shows three major fat boundaries near the top of the image. These appear as bright streaks which grow fainted near the right hand side, especially the second boundary from the top, which appears to grow thinner as it fades out. The ability of different algorithms to enhance this boundary is a good criterion to use in comparing the performance of different detectors.

The results of this work have application beyond the scope of the particular problem the algorithms were designed to solve. Orkisz *et al.* [8] have used a similar technique to enhance visibility of small blood vessels in MR angiography. Moreover, image processing in speckle is itself an area of ongoing concern for many researchers. Notably, Chalana *et al.* [9] and Mikic *et al.* [10] have approached the problem of boundary detection in echo-cardiographic imaging by fitting active contours to the boundaries. That work has met with considerable success, however in both approaches, a human operator is required to identify a starting position for the contour. An algorithm such as that presented here may be able to provide that starting position and more fully automate those procedures.

II. Statistical Line Detection in Speckle Noise

Detection theory is the branch of communication theory which deals with questions of how to optimally determine the presence or absence of a target corrupted by noise. The use of detection theory requires certain insights into the situation at hand; in particular both the target and noise must be well characterized statistically. In the case of ultrasound speckle, the noise's physical cause and statistical behavior are reasonably well understood, and we propose a tractable model for the appearance of the edges. With these statistical tools in place, the detection of boundaries is posed as a composite hypothesis problem which can be handled using techniques found in [11] or [12].

The formulation and analysis of the various detection rules of interest is covered in detail in [7]. To summarize that paper, this section will discuss the statistical distribution of ultrasonic speckle and the form of the composite hypotheses which underlie our detection procedures, and describe the optimal detection rule. In the general correlated speckle case, the optimal rule is computationally intractable, and requires an exact statistical characterization which is usually unavailable. Thus, suboptimal techniques such as the ones described here and in [5] and [7] become attractive because of their computational simplicity.

A. Speckle Statistics

Imaging speckle is a phenomenon which occurs when a coherent source and noncoherent detector are used to interrogate a medium which is rough on the scale of the wavelength. A so-called "fully developed" speckle pattern is formed when each resolution cell contains many point scatterers, none of which produces a significant reflection by itself. The received signal is the superposition of many small reflections whose phases relative to the source are uniformly distributed between zero and 2π over the ensemble of reflections.

The sum of all reflections in each resolution cell can be thought of in terms of a 2-D random walk [13], with the reflection from each scatterer representing a step of a random magnitude and direction. By a central limit theorem argument, the resultant of the random walk can be viewed as a complex Gaussian random variable with independent and identically distributed real and imaginary components. The noncoherent receiver retains only the magnitude of this complex Gaussian variable, and discards the phase. An image is formed by displaying the magnitude of the reflected signal in each resolution cell as a pixel intensity; a fully developed speckle pattern is thus the magnitude of a complex Gaussian field with correlation structure dependent on the pulse shape, the imaging optics, and the distances involved, resulting in a Rayleigh distribution of pixel magnitudes. Notably, to a first approximation, its statistics are independent of the medium being imaged.

If a target is present within a resolution cell, the reflected signal contains a strong coherent component, which provides an offset to the random walk. The resulting pixel appears brighter, and has a Rician distributed intensity. Higher order statistics can be estimated for a speckle pattern by use of the Gaussian moment theorem [14]. A more complete treatment of the statistical properties of ultrasound speckle is found in [7] which draws heavily on material from the classical work of Goodman [13], Burckhardt [15], and Wagner *et al.* [16].

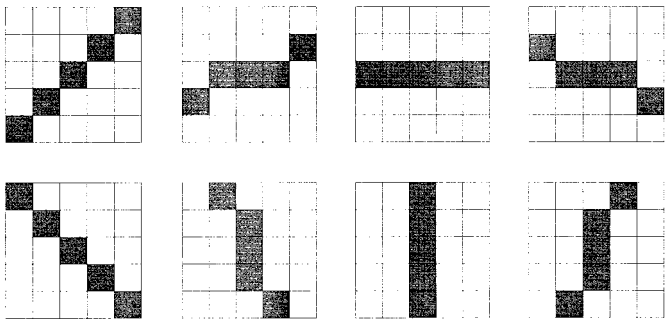

Fig. 2. Set of length five sticks.

B. The Use of "Sticks" in Ultrasound Boundary Detection

The targets of interest do not affect only a single pixel; their effect is along curves which lie on the 3-D surface in view. We have found [5], [6], [17] that a set of "sticks," short line segments of variable orientation, can effectively model these targets in a statistical sense. Intuitively, this is a very satisfying notion; large scale linear image features will line up with a stick of sufficiently short length, while speckle will not if the stick is sufficiently long. Fig. 2 shows a set of sticks of length five. There are many possible discretizations of the set of lines passing through a region; the square support of the templates in Fig. 2 was selected because it can be easily resized to larger or smaller scales. In the following sections, the sticks will be used as templates in a composite hypothesis test, the result of which will indicate which (if any) stick is present passing through each point in an image.

The technique used here is related to the class of "rotating kernel min–max transformation" investigated by Lee and Rhodes [18]–[21] and Hou and Bamberger [22], [23], but to our knowledge, our work is the first application of this idea to medical imaging [5]. Other researchers have considered detection issues in ultrasound and other speckle imaging modalities, but have generally restricted their attention to the identification of more generally shaped image *regions* of contrasting statistical behavior [4], [24]–[26], and are thus less appropriate for the problem of detecting the linear features which characterize abrupt tissue discontinuities.

C. Optimal Detection

Optimal detection in the maximum-likelihood sense is the formulation of a mathematical rule to indicate that a target is present within a signal or that the signal is more likely just noise. The rule is obtained by comparing the conditional probability density functions (pdfs) under the active (signal present) and null (noise only) hypotheses, to determine which is the more likely state of nature underlying the observation. For example, if signal $\mathbf{x}$ is received, and

$$\begin{aligned}&\text{Prob}\left[\text{Receive}\,\mathbf{x}\,|\,\text{target present}\right]\\&\quad>\text{Prob}\left[\text{Receive}\,\mathbf{x}\,|\,\text{no target present}\right]\end{aligned}\tag{1}$$

then it is statistically likely that a target is present. This test is equivalent to computing a *likelihood ratio* of conditional pdf's, and comparing the resulting function to a threshold.

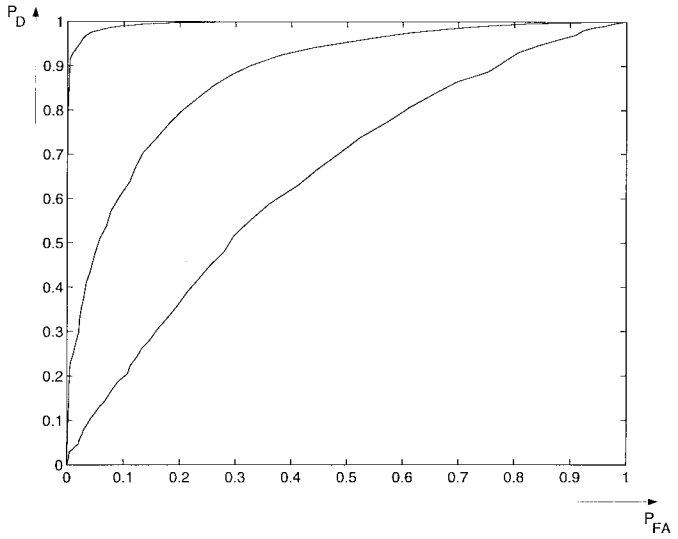

(a)

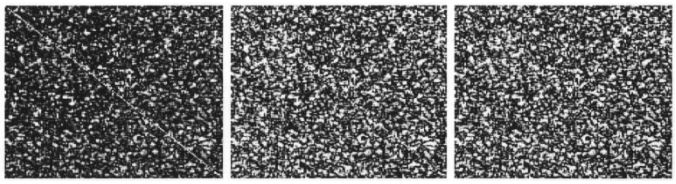

(b)

Fig. 3. (a) ROC curves for the Sticks detection rule in simulated correlated speckle of three different power levels and (b) sample signal and noise realizations at each signal level. The signal appears in each simulated image as a thin diagonal line from upper left to lower right. These signal levels are intended to represent, from left to right, high to low SNR relative to typical medical ultrasound image quality. This figure is a composite of data which appear in [7].

In some cases such as binary detection in Gaussian noise, the likelihood ratio function can be simplified, leading to a low-order optimal test.

In the multiple hypothesis case the likelihood ratio is more complicated because the active hypothesis has several different forms which leads to a sum of conditional pdfs, weighted by the prior probability of each hypothesis

$$\begin{aligned}\Lambda_{\text{LRT}}(\mathbf{x})&=\frac{\text{Prob}\left[\text{Receive}\,\mathbf{x}\,|\,\text{target present}\right]}{\text{Prob}\left[\text{Receive}\,\mathbf{x}\,|\,\text{no target present}\right]}\\&=\frac{\sum_i \pi_i\,\text{Prob}\left[\text{Receive}\,\mathbf{x}\,|\,i\text{th target present}\right]}{\pi_0\,\text{Prob}\left[\text{Receive}\,\mathbf{x}\,|\,\text{no target present}\right]}\end{aligned}\tag{2}$$

where π_i is the prior probability that hypothesis i occurs. The decomposition of the target present probability into the sum in (2) follows from our premise that the stick orientations are a mutually exclusive and exhaustive [27] representation of the possible lines passing through each image pixel.

1) Linear Stick Detection: The optimal detection rule is computationally infeasible and requires clairvoyant knowledge of the noise statistics. As an alternative, we have developed the Sticks technique, a simpler method which is more robust in the face of imperfectly characterized noise, but whose performance can approach the optimal in the case of minimally correlated speckle (i.e., obtained from an underlying white

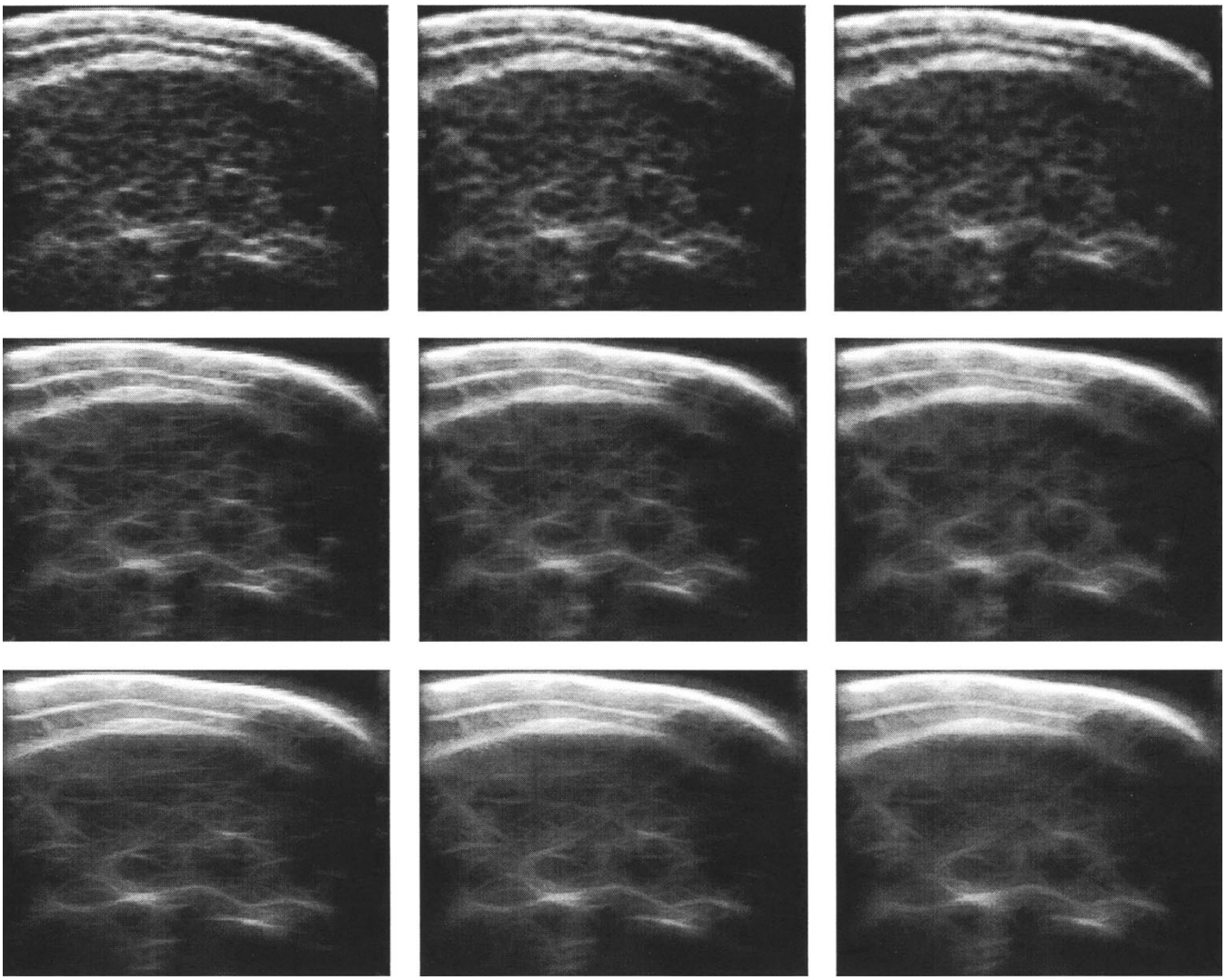

Fig. 4. Composite of images processed with sticks of varying lengths and thicknesses. Length varies from seven to 15 to 23 from left to right; thickness varies from one to three to five from top to bottom (image cropped to show detail).

complex Gaussian field). This technique is implemented by overlaying each orientation stick above a point and adding pixel which lie along the stick. The maximum value over all orientations is retained as the test statistic for that point. This approach is similar to the Hough transform [28], which is widely used to detect lines in computer vision applications.

The Sticks technique is an implementation of the GLRT for short line segments in an additive, white Gaussian noise field. While this is clearly an incorrect statistical model for speckle noise, it is reminiscent of Smith *et al.* [24] who use the sum of values from *independent* correlation cells within a lesion as a reasonable approximation to the solution of the exact detection problem which requires the decomposition of the image into uncorrelated components [13].

The effect of summing correlated pixel (as we do here) is studied in [7] where the Sticks detector is compared in performance with a Sticks detector preceded by a prewhitening operation. The whitening was shown to produce nearly optimal performance in ROC analysis of Monte Carlo simulations, however the estimation of the whitening filter in real images has proven elusive. Nevertheless, when the stick size is significantly larger than the speckle correlation length, we expect that the support of each stick will include several independent correlation cells, the sum over which will be related to the sum over the independent correlation cells alone.

Fig. 3(a) shows a set of receiver operating characteristic (ROC) curves corresponding to Sticks detection in correlated speckle of three different power levels. A simulated ultrasound scan showing a noise realization at each power level is shown in Fig. 3(b). In each of these images, a simulated target is found along the diagonal from upper left to lower right. This figure is a composite of curves and images which appear in [7]. An ROC study of performance of the Sticks algorithm in real images is beyond the scope of this paper, but Fig. 3 gives an indication of the performance that might be expected at different noise levels.

III. Effect of Stick Length and Thickness

The implementation of the Sticks technique requires a tradeoff between effective line enhancement and good speckle reduction. To obtain good results, the sticks should be made

longer than the correlation length of the noise, yet shorter than the distance over which the boundaries appear to be straight lines. A longer stick achieves greater speckle suppression at the expense of a weaker match with more tightly curving boundaries; similarly, "fatter" sticks are more sensitive than thinner sticks to broad but dim boundaries.

Fig. 4 shows the effects of varying stick length between seven, 15, and 23 pixels, and stick thickness between one, three, and five pixels. The longer sticks have the effect of blurring the speckle in the interior of the muscle, while more clearly emphasizing the boundaries between fat layers and the muscle. However, these effects come at the expense of visibility of certain image features, such as the thin boundary between the fat layers in the upper right corner of the image. Increasing stick thickness has the effect of enhancing the relative brightness of the broad boundaries, while introducing some blur in the transitions between boundary and off-boundary pixel. More importantly, the use of thicker sticks makes very thin boundaries less visible.

These effects can be more quantitatively studied by considering the statistics of the stick operator output. Ideally, we hope to obtain a large valued, low variance output when a target is present and a small valued, low variance output when no target is present. The following index of performance is maximized under these circumstances

$$D(N, M) = \frac{E[Y(N, M) - Y(N, 0)]^2}{\max\Big(\mathrm{var}\big(Y(N, M)\big), \mathrm{var}\big(Y(N, 0)\big)\Big)} = \frac{E[Y(N, M) - Y(N, 0)]^2}{\mathrm{var}\big(Y(N, M)\big)} \tag{3}$$

where

$$Y(N, M) = \frac{1}{\sqrt{N}}\left[\sum_{i=1}^{M} x_1(i) + \sum_{j=1}^{N-M} x_0(j)\right]. \tag{4}$$

The quantity $Y(N, M)$ is the projection of an idealized image onto a size N stick of normalized energy, i.e., one containing N points, each of value $N^{-1/2}$. The quantity $Y(N, M)$ is the sum of pixel intensities from M true target points and $N - M$ pure noise points, corresponding to partial overlap of a stick detection template with a target. Detection with a stick perfectly fit to the target is indicated by $Y(N, N)$, while the stick output under the null hypothesis is $Y(N, 0)$.

In additive white Gaussian noise, the quantity $D(N, M)$ can be interpreted as a signal-to-noise ratio (SNR), since it is proportional to the square of the expected difference in stick output under active and null hypotheses, and inversely proportional to the variance under the active hypothesis. In fully developed speckle, $D(N, M)$ is still a reasonable performance index because it requires only low-order moments which can be reliably estimated [29]. Smith *et al.* [24] use a similar measure which they call "optimal signal-to-noise ratio" to derive a detector for image regions which are bright due to the presence of lesions. This statistic is also related to deflection [30], which is used as a criterion for the design of optimal linear-quadratic detection rules for use in ultrasound speckle in [7], and also to the "contrast" [13] of the speckle pattern, which has been used in ultrasound tissue characterization (for example, in [31] and [32]).

Brown *et al.* [33] have shown that the use of SNR statistics such as (3) may be an unreliable indicator of detector power for non-Gaussian noise, especially in instances of high signal strength. This index must thus be validated for the noise distribution in question. Results in [7] indicate that in simulated speckle deriving from an uncorrelated Gaussian distribution, the Sticks detector is nearly equal in performance to the optimal detector, and that in correlated speckle, a prewhitening operation allows Sticks to perform close to optimally. These are essentially matched filter techniques, which are optimal in Gaussian noise because they maximize SNR; their success in detecting lines in non-Gaussian simulated speckle leads us to believe that SNR measures such as (3) may accurately be used in this context to quantify detector power, in spite of their general suboptimality for this purpose.

If the speckle is assumed to be described by Rayleigh/Rician statistics, the mean and second moment of $Y(N, M)$ are given by

$$E[Y(N, M)] = \frac{1}{\sqrt{N}} E\left[\sum_{i=1}^{M} x_1(i) + \sum_{j=1}^{N-M} x_0(j)\right] = \frac{M\mu_1 + (N-M)\mu_0}{\sqrt{N}} \tag{5}$$

and

$$\begin{aligned} E[Y(N, M)^2] &= \frac{1}{N} E\left[\left(\sum_{i=1}^{M} x_1(i) + \sum_{j=1}^{N-M} x_0(j)\right)^2\right] \\ &= \frac{1}{N} E\left[\left(\sum_{i=1}^{M} x_1(i)\right)^2 + 2\left(\sum_{i=1}^{M} x_1(i)\right) \cdot \left(\sum_{j=1}^{N-M} x_0(j)\right) + \left(\sum_{j=1}^{N-M} x_0(j)\right)^2\right] \\ &= \frac{1}{N}\Big(\big\{ME\big[x_1^2\big] + M(M-1)E[x_1]^2\big\} \\ &\quad + 2(N-M)ME[x_1]E[x_0] \\ &\quad + \big\{(N-M)E\big[x_0^2\big] \\ &\quad + (N-M)(N-M-1)E[x_0]^2\big\}\Big) \\ &= \frac{1}{N}\big(M\sigma_1^2 + M^2\mu_1^2 + (N-M)\sigma_0^2 \\ &\quad + (N-M)^2\mu_0^2 + 2(N-M)M\mu_0\mu_1\big) \end{aligned} \tag{6}$$

where μ_1 and σ_1^2 are the mean and variance of target points in the image, and μ_0, and σ_0^2 are the mean and variance of noise-only points. These statistics can be calculated by application of the Gaussian moment theorem in terms of the underlying Gaussian random field statistics.

The variance of $Y(N, M)$ is then

$$\begin{aligned}\operatorname{var}[Y(N,M)] &= E\left[Y(N,M)^2\right] - E\left[Y(N,M)\right]^2 \\ &= \frac{1}{N}\left[M\sigma_1^2 + M^2\mu_1^2 + (N-M)\sigma_0^2 \right. \\ &\quad + (N-M)^2\mu_0^2 + 2(N-M)M\mu_0\mu_1 \\ &\quad - \left(M^2\mu_1^2 + 2(N-M)M\mu_0\mu_1 \right. \\ &\quad \left.\left. + (N-M)^2\mu_0^2\right)\right] \\ &= \frac{M\sigma_1^2 + (N-M)\sigma_0^2}{N}. \end{aligned} \tag{7}$$

Note that because $\sigma_1 > \sigma_0$

$$Y(N, M) \geq Y(N, 0) \tag{8}$$

for all positive M, which simplifies the denominator of (3)

$$\begin{aligned} D(N,M) &= \frac{E[Y(N,M) - Y(N,0)]^2}{\operatorname{var}(Y(N,M))} \\ &= \frac{\left(M\mu_1 + (N-M)\mu_0\right)^2/N}{\left(M\sigma_1^2 + (N-M)\sigma_0^2\right)/N} \\ &= \frac{\left(M\mu_1 + (N-M)\mu_0\right)^2}{\left(M\sigma_1^2 + (N-M)\sigma_0^2\right)}. \end{aligned} \tag{9}$$

For a given target size, $D(N, M)$ increases linearly with increasing stick length, reaching a maximum value when the stick exactly matches the target. When the stick is larger than the target, increases in stick size can only extend the operator to include pure noise. This results in an increase in M, and a constant value of N, leading to a decrease in $D(N, M)$. The value of $D(N, M)$ is plotted for targets of varying length in 5.2 dB noise in Fig. 5. The figure shows the costs of under- or over-estimating the target size when selecting a stick length and thickness. While the costs of under-estimation appear more significant, the penalty for over-estimation still must not be ignored. Since stick length and thickness are generally set once for an entire image, care must be taken to ensure that an appropriate value is selected. The potential exists for an adaptive size stick or sequential detection at multiple scales, however these topics are beyond the scope of the present paper.

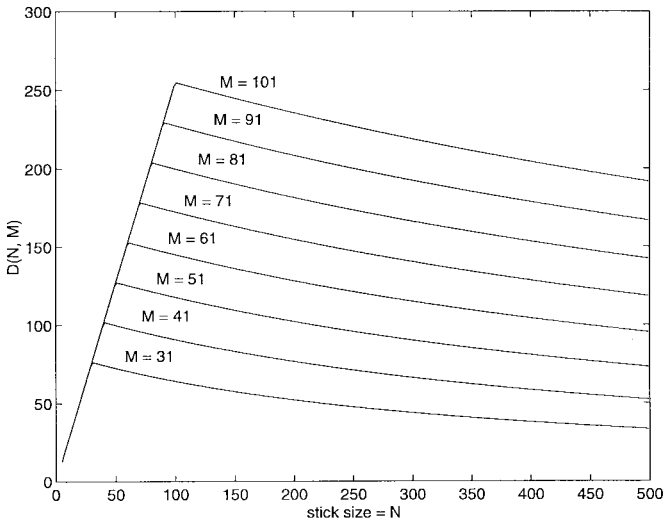

Fig. 5. $D(N, M)$ for targets of indicated length in 5.2-dB simulated speckle. As stick size increases up to the target length, $D(N, M)$ increases linearly; when stick size is larger than the target size, $D(N, M)$ decreases, indicating optimal performance when the stick is well matched to the target.

(a)

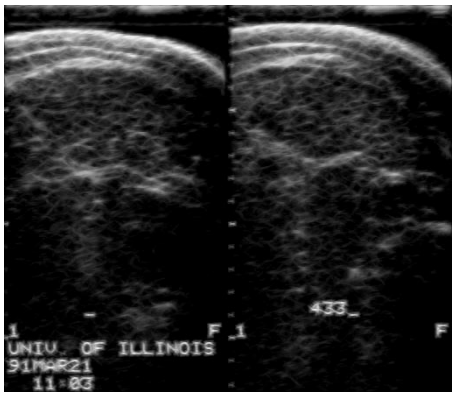

(b)

Fig. 6. Original image processed with: (a) length seven, thickness one sticks and (b) length seven, thickness one decision-directed sticks procedure.

IV. Decision-Directed Sticks

Implicitly, the techniques described above have assumed that the boundaries are uniformly distributed in their orientation. For the case of medical ultrasound, this is an unwarranted simplification, because the modality is physically incapable of imaging structures which lie parallel to the interrogating sound beam. In fact, almost all the boundaries in an acoustic image will be oriented nearly perpendicular to the beam direction.

Inclusion of a set of prior probabilities for the line orientation in the detection rule can greatly improve on the performance of the GLRT. The GLRT is similar to a likelihood ratio test (2), except that the numerator

$$\text{LRT}(\mathbf{x}) \sim \sum_i \pi_i \text{Prob}\left[\text{Receive } \mathbf{x} \,\middle|\, i\text{th target present}\right] \tag{10}$$

is replaced with conditional pdf for the maximum likelihood hypothesis

$$\text{GLRT}(\mathbf{x}) \sim \max_i \text{Prob}\left[\text{Receive}\,\mathbf{x}\,|\,i\text{th target present}\right]. \quad (11)$$

It is most useful when the prior π_i are unknown. If the priors are known or can be estimated, however, we can replace the maximum likelihood estimate in (11) with a more powerful maximum *a posteriori* estimate. We call the resulting test the decision-directed Sticks detector

$$\text{DDS}(\mathbf{x}) \sim \max_i \pi_i \,\text{Prob}\left[\text{Receive}\,\mathbf{x}\,|\,i\text{th target present}\right]. \quad (12)$$

The new test can be implemented by thresholds

$$\begin{aligned}\gamma &= \max_i \frac{\pi_i\, p_{r\,|\,H_i}(\mathbf{x}\,|\,H_i)}{\pi_0\, p_{r\,|\,H_0}(\mathbf{x}\,|\,H_0)} \\ &\approx \frac{1}{\pi_0}\max_i \frac{\pi_i \exp\left(-\frac{1}{2\sigma^2}(\mathbf{x}-\mu_i)^T(\mathbf{x}-\mu_i)\right)}{\exp\left(-\frac{1}{2\sigma^2}\mathbf{x}^T\mathbf{x}\right)} \\ &\propto \max_i \pi_i \exp\left(\frac{1}{\sigma^2}\langle \mathbf{x},\,\mu_i\rangle + -\frac{1}{2\sigma^2}\langle \mu_i,\,\mu_i\rangle\right) \\ &= C \max_i \exp\left(\log \pi_i + \frac{1}{\sigma^2}\langle \mathbf{x},\,\mu_i\rangle\right) \\ &\propto \max_i \left(\log \pi_i + \frac{1}{\sigma^2}\langle \mathbf{x},\,\mu_i\rangle\right) \end{aligned} \quad (13)$$

where $\langle\cdot,\,\cdot\rangle$ denotes an inner product, μ_i denotes the ith target, and σ^2 is the variance of the noise, assumed to be white and Gaussian, and $C = \pi_i \exp\left(-1/2\sigma^2\langle\mu_i,\,\mu_i\rangle\right)$, a constant with respect to i, since all the sticks are the same length and have equal energy. Note that since $0 \le \pi_i \le 1$, it is known that $\log \pi_i \le 0$; thus the prior term in (13) is a penalty on less probable orientations. Furthermore, the penalty is possibly quite stiff, since $\lim_{x\to 0} \log x = -\infty$.

The division of the projection value by the noise variance has an additional interpretation: the prior information attains greater significance in higher noise levels when the projection is highly noisy. Conversely, when the noise level is lower, the projection information is given more weight. In the case of very high SNR, the test reduces to the original Sticks algorithm. If μ_i has values zero or $N^{-1/2}$, as in the formulation we have used for line detection, (13) reduces to the selection of the line sum with the maximum value after a penalty has been applied to terms unlikely to be true lines. The original Sticks algorithm is obtained as a special case by assuming equal priors, or when the SNR is very high.

Even though ultrasound is most sensitive to targets oriented perpendicular to the beam axis, the exact reflection coefficient as a function of incidence angle can not be known *a priori.* Thus, it is not possible to infer a set of prior probabilities from scanning geometry alone. This is especially true if the image is composed from scans taken from different locations averaged to reduce speckle intensity. Furthermore, in more general imaging problems, for example in MR angiography [8], the scanning geometry may not produce any preferred line orientation at all.

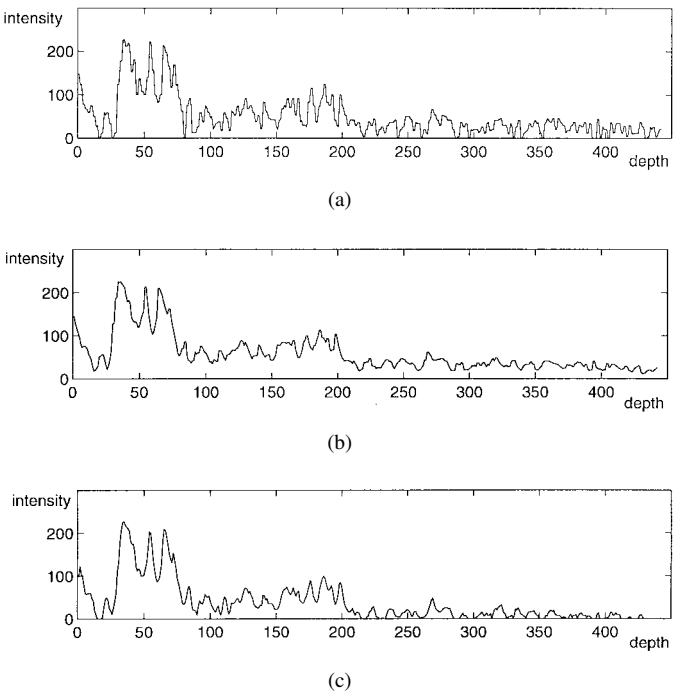

Fig. 7. (a) Vertical cross sections of the original image, (b) the processed images in Fig. 6: length seven, thickness one sticks, and (c) length seven, thickness one decision directed sticks. Both processing algorithms are effective at reducing noise and making boundary peaks more easily detectable, especially the decision-directed approach in (c).

For these reasons, it is desirable to estimate the prior from the image itself. In [34], we presented the following method of performing this estimation. First, the Sticks algorithm is used to determine the angle of the most prominent line segment passing through each point. Next, a histogram is formed of the angles near each pixel (e.g., within the support of the stick operators). This histogram is normalized to unit volume and used as a prior distribution on line segments passing through the point. This technique is inspired by the treatment of maximum *a posteriori* probability estimation in [35].

The decision-directed Sticks algorithm can thus be written in three steps [34]: the determination of the most probable line direction at each point, the computation of a prior probability for each angle at each point, and the computation of the final test statistic

$$\alpha(x,\,y) = \arg\max_\theta \sum_{i,\,j} s_\theta(i,\,j) f(x-i,\,y-j) \quad (14)$$

$$\pi_\theta(x,\,y) = \sum_{i,\,j} w(x+i,\,y+j) I\big(\alpha(x,\,y)=\theta\big) \quad (15)$$

$$f'(x,\,y) = \max_{\theta_i} \left(\log \pi_\theta(x,\,y) + \frac{1}{\sigma^2} \cdot \sum_{i,\,j} s_\theta(i,\,j) f(x-i,\,y-j)\right) \quad (16)$$

where $f(x,\,y)$ is the original image and $f'(x,\,y)$ denotes the output test statistic, $\alpha(x,\,y)$ denotes the most probable line orientation at point $(x,\,y)$, $s_\theta(i,\,j)$ is a stick at the θ orientation, $w(x,\,y)$ is a mask function which is unit valued on the union of the support of the sticks and zero-valued

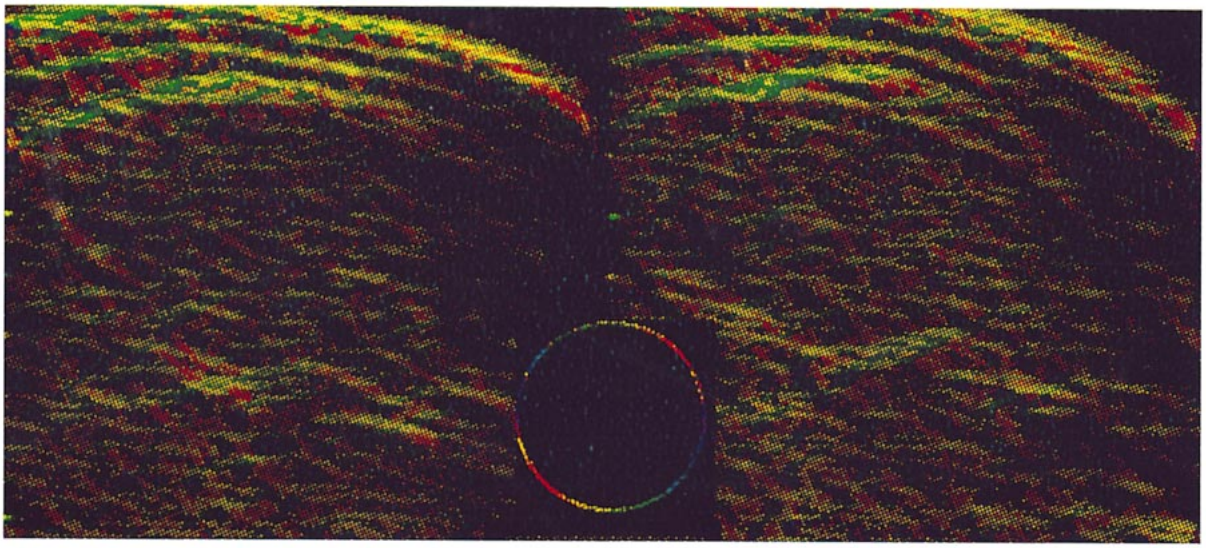

(a)

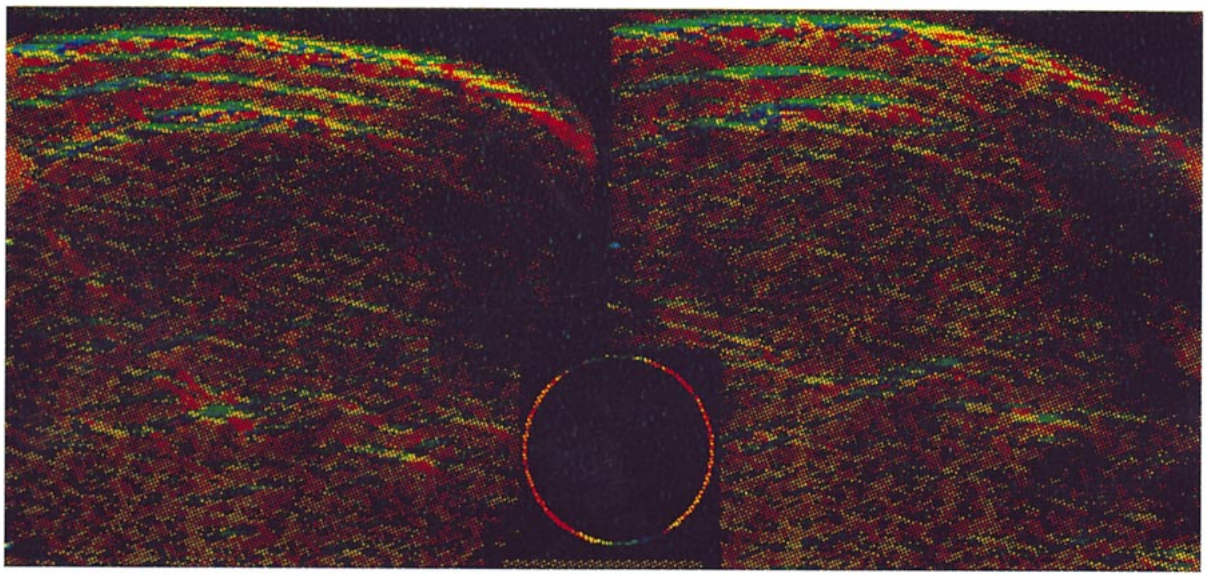

(b)

Fig. 8. Original image with false color applied to indicate the direction of the most prominent stick at each point. The hue applied is obtained from the direction of the most prominent length 15, thickness one sticks at each point. The colored circle visible in the image was superimposed on the raw image and processed along with the rest of the image; its color at various points on its diameter indicates the hue assigned to boundaries at corresponding orientations. The image shows a range of hues along curving lines, such as the fat boundaries near the top of the image. Image (a) is obtained by distributing hues evenly about the color circle and (b) is the result of warping the color map to show a full spectrum along the broad boundary at the top of the image.

elsewhere, $\pi_\theta(x, y)$ is the computed probability of a line at orientation θ at point (x, y), and $I(expr)$ is the indicator function, equal to one, if $\exp r$ is true; zero, if false.

Fig. 6(a) shows the image from Fig. 1 processed with a length seven, thickness one decision-directed sticks procedure. Note the thin boundary between the two layers of subcutaneous fat which is emphasized even though it is only a few pixel wide. This is characteristic of the ability of all the sticks techniques to connect image lines while rejecting the darker areas between the lines. This tendency can be seen in the processed text, where connections are made between letters and between unconnected parts of letters. This is not a serious limitation in medical imaging where tightly curving features such as lettering are uncommon. The lettering does, however, provide a convenient means to demonstrate the improvement of decision directed sticks over sticks projection [Fig. 6(b)]: in addition to yielding more sharply defined boundaries and greater noise suppression, the artifacts surrounding the lettering are far less pronounced in Fig. 6(a) than in (b).

A vertical slice of each of these images is shown in Fig. 7, which shows the improvement in peak detectability and noise rejection of the sticks and decision directed sticks procedures. In Fig. 7(b) and (c) the boundaries are marked by narrower peaks, and the nonboundary points by lower intensity, especially in the decision-directed Sticks image slice, Fig. 7(c).

V. Image Enhancement with False Color

False color is frequently used in computed imaging systems as a means of supplementing the information content of a gray-scale display, for example in Doppler ultrasonics to display direction and velocity of blood flow. In the techniques described thus far, output images have been displayed in gray-scale only. In this section, we propose to use false color to display the *orientation* of the stick which produced the maximum projection, in addition to the maximum projection value itself. This can be accomplished by assigning each pixel an orientation dependent hue, and should result in improved visibility of boundaries.

The idea of applying false color to an ultrasound image was used in [36] to display statistical properties of the backscatter at each point. We feel the notion has broad applicability in ultrasound image enhancement, and in particular that false color can significantly improve the detectability of weak features by providing image detail that otherwise would not be seen. As was the case with the orientation estimation in the decision directed Sticks procedure, the use of false color to display angle information can be used in conjunction with any Sticks or similar technique.

The problem of displaying angle and intensity as a color is one of displaying a hue, saturation, and intensity (HSV) color space. This is complicated, because while HSV is a natural space for describing perceptible colors, not every HSV triplet can be made up out of the red, green, and blue (RGB) components which compose standard computer displays. Thus, the mapping from HSV to RGB space is not exact or unique. Fig. 8 was produced using the procedure shown in Fig. 9.

```
function (h, s, v) → (r, g, b)

h = h / 60
i = floor (i)
f = h - i
p = v*(1 - s)
q = v*(1 - s*f)
t = v*(1 - s*(1 - f))
case i of
        0: (r, g, b) = (v, t, p)
        1: (r, g, b) = (q, v, p)
        2: (r, g, b) = (p, v, t)
        3: (r, g, b) = (p, q, v)
        4: (r, g, b) = (t, p, v)
        5: (r, g, b) = (v, p, q)
end
```

Notes:
h is an angle between 0° and 360°.
s is the saturation value set to some constant between zero and one (unused in this application).
Value is normalized to lie between zero and one.
Outputs r, g, and b all fall between zero and one.

Fig. 9. Conversion from (H, S, V) to (R, G, B) color space. Adapted from [37].

Example images resulting from enhancement with false color are shown in Figs. 8 and 10. These figures show the original image and the Sticks output image in false color obtained by coding the orientation of length 15, thickness one sticks as a hue. Note that the uncolored images can be obtained from the colored ones by summing red, green and blue components and normalizing to suit the display's dynamic range. In clinical applications, the ability to display additional information without "corrupting" the original image is important because the expertise of the ultrasound sonographers is highly specialized in analyzing images with standard appearance.

Figs. 8(a) and 10(a) show the raw false color images, where hue is equally distributed over all angles. Figs. 8(b) and 10(b) show the same images, but with a color map which shows almost a full spectrum of color in the range of angles which describe the fat boundaries near the top of the image. The colored circle visible in the image was superimposed on the raw image and processed along with the rest of the image; its color at various points on its diameter indicates the hue assigned to boundaries at corresponding orientations.

The colored images, especially the (b) images, show clearly that the outermost fat boundary is in actuality two separate boundaries, a fact which is much more visually apparent than in the corresponding gray-scale images. The visibility of the boundaries is further improved by the fact that the area between boundaries is assigned a contrasting color. This is because sticks oriented perpendicular to the boundaries are selected in this region in an attempt by the algorithm to capture boundary energy to display at these points. In a gray-scale display, some of these points might erroneously appear to be part of the boundaries; with false color, their distinctness is clear.

We believe that the use of false color is a very promising technique with potential to significantly improve the capability of diagnostic imaging devices. False color allows two additional degrees of freedom in the display (only one of which is used here), which can be used to supply additional information to the user. Most importantly, the additional information can be introduced into the display or switched off without qualitatively changing the appearance of the scan. Further research is required to determine the best quantities to encode using false color.

VI. Conclusion

This paper has discussed the use of the Sticks algorithm to enhance images for boundary detection. The technique operates by applying a set of templates as a filter bank, and retaining the largest filter output at each point as a test statistic. It has been shown that by modifying the length and thickness of the templates, the technique can be made more sensitive to thicker lines, or achieve a different trade off between speckle suppression and the ability to follow tightly curving boundaries. We have also demonstrated a technique

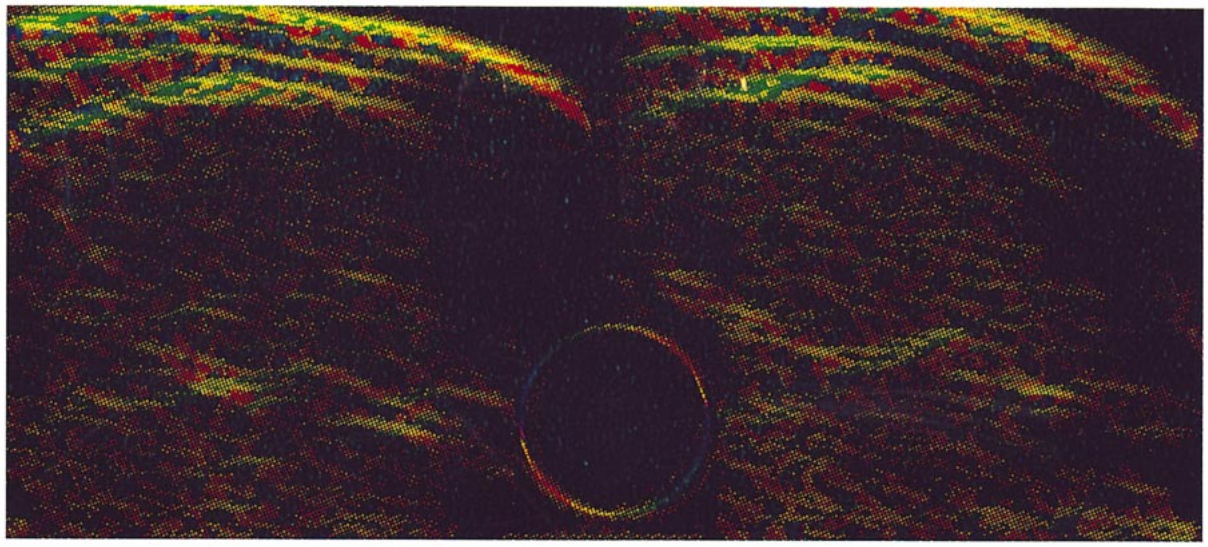

(a)

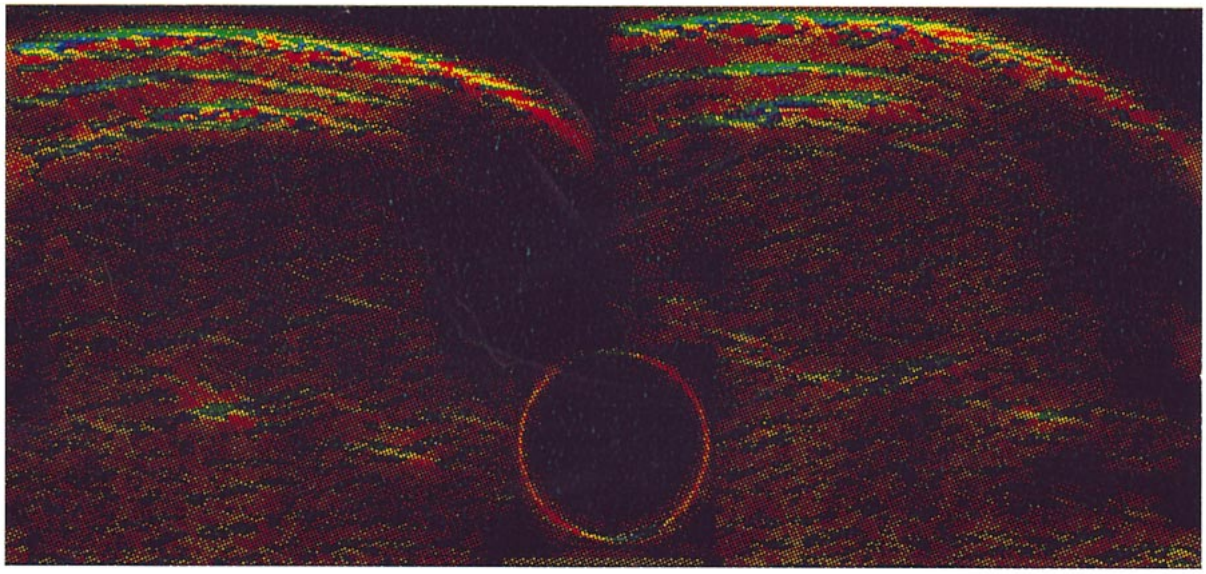

(b)

Fig. 10. Sticks image with false color applied to indicate the direction of the most prominent stick at each point. The hue applied is obtained from the direction of the most prominent length 15, thickness one sticks at each point. The colored circle visible in the image was superimposed on the raw image and processed along with the rest of the image; its color at various points on its diameter indicates the hue assigned to boundaries at corresponding orientations. The image shows a range of hues along curving lines, such as the fat boundaries near the top of the image. Image (a) is obtained by distributing hues evenly about the color circle and (b) is the result of warping the color map to show a full spectrum along the broad boundary at the top of the image.

for using the image itself to estimate the prior probability of a line of any orientation passing through each point, which results in greater speckle rejection and better performance of the detection procedure. Finally, we have presented a means of displaying the angle information at each point as a false color. This is an extremely promising idea because it allows for entirely new information to be incorporated into an image without affecting the gray level value of the original image.

Note that the class of rotating kernel detectors to which these algorithms belong is far broader than that which can be surveyed here. Lee and Rhodes [18]–[21] and Hou and Bamberger [22], [23] have experimented with similar approaches. In our own work, we have used the median operation [6] in place of a sum, and obtained results similar to those produced by the Sticks algorithm. These methods have applicability in medical ultrasound imaging because of their ability to enhance the linear image features which correspond to tissue boundaries. They also may find applicability in other forms of coherent imaging, such as microwave synthetic aperture imaging, because of the statistical and physical analogy between the speckle noise in these two imaging modalities.

ACKNOWLEDGMENT

The authors would like to thank I. Hein, N. B. Smith, W. D. O'Brien, Jr., and J. Novakofski for the pig image.

REFERENCES

[1] R. F. Wagner, M. F. Insana, and S. W. Smith, "Fundamental correlation lengths of coherent speckle in medical ultrasonic images," *IEEE Trans. Ultrason., Ferroelect., Freq. Contr.,* vol. 35, pp. 34–44, Jan. 1988.

[2] J. Canny, "A computational approach to edge detection," *IEEE Trans. Pattern Anal. Machine Intell.,* vol. PAMI-8, pp. 679–698, Nov. 1986.

[3] R. C. Gonzalez and R. E. Woods, *Digital Image Processing.* Reading, MA: Addison-Wesley, 1992.

[4] A. C. Bovik, "On detecting edges in speckle imagery," *IEEE Trans. Signal Processing,* vol. 36, pp. 1618–1627, Oct. 1988.

[5] R. N. Czerwinski, D. L. Jones, and W. D. O'Brien, Jr., "An approach to boundary detection in ultrasound imaging," presented at *1993 IEEE Ultrasonics Symp.,* Baltimore, MD, Nov. 1993.

[6] ———, "Ultrasound speckle reduction by directional median filtering," presented at IEEE Int. Conf. Image Processing—CIP'95, Washington, DC, Oct. 1995.

[7] ———, "Line and boundary detection in speckle images," *IEEE Trans. Image Processing,* vol. 7, pp. 1700–1714, Dec. 1998.

[8] M. M. Orkisz, C. Bresson, I. E. Magnin, 0. Champin, and P. C. Douek, "Improved vessel visualization in MR angiography by nonlinear anisotropic filtering," *Magn. Reson. Med.,* vol. 37, pp. 914–919, 1997.

[9] V. Chalana, D. Linker, D. R. Haynor, and Y. Kim, "A multiple active contour model for cardiac boundary detection on echographic sequences," *IEEE Trans. Med. Imag.,* vol. 15, pp. 290–298, June 1996.

[10] I. Mikic, S. Krucinski, and J. D. Thomas, "Segmentation and tracking of mitral valve leaflets in echocardiographic sequences: Active contours guided by optical flow estimates," in *Proc. SPIE—Medical Imaging 1996: Image Processing,* vol. 2710, M. H. Loew and K. M. Hanson, Eds., 1996, p. 311.

[11] H. V. Poor, *An Introduction to Signal Detection and Estimation.* New York: Springer-Verlag, 1988.

[12] H. L. Van Trees, *Detection, Estimation, and Modulation Theory—Part I.* New York: Wiley, 1968.

[13] J. W. Goodman, "Statistical properties of laser speckle patterns," in *Laser Speckle and Related Phenomena,* J. C. Dainty, Ed. Berlin, Germany: Springer-Verlag, 1977, no. 9, ch. 2, pp. 9–77; in Topics in Applied Physics.

[14] K. S. Miller, *Complex Stochastic Processes.* Reading, MA: Addison-Wesley, 1974.

[15] C. B. Burckhardt, "Speckle in ultrasound B-mode scans," *IEEE Trans. Sonics Ultrason.,* vol. SU-25, no. 1, pp. 1–6, Jan. 1978.

[16] R. F. Wagner, S. W. Smith, J. M. Sandrik, and H. Lopez, "Statistics of speckle in ultrasound B-scans," *IEEE Trans. Sonics Ultrason.,* vol. 30, no. 3, pp. 156–163, May 1983.

[17] R. N. Czerwinski, D. L. Jones, and W. D. O'Brien, Jr., "A comparison of detection rules for lines and boundaries in acoustic speckle," presented at 22nd Int. Symp. Acoustic Imaging, Florence, Italy, Sept. 1995.

[18] Y. K. Lee and W. T. Rhodes, "Feature detection and enhancement by a rotating kernel min–max transformation," in *Proc. SPIE —Hybrid Image and Signal Processing—Part II,* vol. 1297, F. T. Luk, Ed., 1990, pp. 154–159.

[19] ———, "Scale- and rotation-invariant pattern recognition by a rotating kernel min–max transformation," in *Proc. SPIE—Optical Information-Processing Systems and Architectures—Part II,* vol. 1347, F. T. Luk, Ed., 1990, pp. 146–155.

[20] ———, "Nonlinear image processing by a rotating kernel transformation," *Opt. Lett.,* vol. 15, no. 23, pp. 1383–1385, Dec. 1990.

[21] ———, "Invariant pattern recognition using angular signature functions," *Appl. Opt.,* vol. 32, no. 23, pp. 4372–4377, Aug. 10, 1993.

[22] J. Hou and R. Bamberger, "Orientation selective operators for ridge, valley, edge, and line detection in imagery," in *Proc. IEEE Int. Conf. Acoustics, Speech and Signal Processing—ICASSP'94,* Adelaide, Australia, May 1994, pp. V-25–V-28.

[23] ———, "A robust system for lineament analysis of aero-magnetic imagery using orientation analysis and edge linking," in *Proc. IEEE Int. Conf. Image Processing—ICIP'94,* Austin, TX, Nov. 1994, pp. I-963–I-967.

[24] S. W. Smith, R. F. Wagner, J. M. Sandrick, and H. Lopez, "Low contrast detectability and contrast/detail analysis in medical ultrasound," *IEEE Trans. Sonics Ultrason.,* vol. SU-30, no. 3, pp. 164–173, May 1983.

[25] K. D. Donohue, M. Rahmati, L. G. Hassebrook, and P. Gopalakrishnan, "Parametric and nonparametric edge detection for speckle degraded images," *Opt. Eng.,* vol. 32, no. 8, pp. 1935–1946, Aug. 1993.

[26] A. C. Bovik and D. C. Munson, Jr., "Boundary detection in speckle images," in *Proc. IEEE Int. Conf. Acoustics, Speech and Signal Processing—ICASSP'85,* Tampa, FL, 1985, pp. 893–896.

[27] H. Stark and J. W. Woods, *Probability, Random Processes, and Estimation Theory for Engineers.* Englewood Cliffs, NJ: Prentice-Hall, 1986.

[28] R. 0. Duda and P. E. Hart, "Use of the Hough transform to detect lines and curves in pictures," *Commun. ACM,* vol. 15, no. 1, pp. 11–15, Jan. 1972.

[29] R. N. Czerwinski, "Boundary detection in ultrasonic speckle," Ph.D. dissertation, Univ. Illinois at Urbana-Champaign, 1996.

[30] B. Picinbono and P. Duvaut, "Optimal linear-quadratic systems for detection and estimation," *IEEE Trans. Inform. Theory,* vol. 34, pp. 304–311, Mar. 1988.

[31] T. A. Tuthill, R. H. Sperry, and K. J. Parker, "Deviations from Rayleigh statistics in ultrasonic speckle," *Ultrason. Imag.,* vol. 10, no. 1, pp. 81–89, Jan. 1988.

[32] G. E. Sleefe and P. P. Lele, "Tissue characterization based on scatterer number density estimation," *IEEE Trans. Ultrason., Ferroelect., Freq. Contr.,* vol. 35, no. 6, pp. 749–757, Nov. 1988.

[33] D. G. Brown, M. F. Insana, and M. Tapiovaara, "Detection performance of the ideal decision function and its Maclaurin expansion: Signal position unknown," *J. Acoust. Soc. Amer.,* vol. 97, no. 1, pp. 379–398, Jan. 1995.

[34] R. N. Czerwinski, D. L. Jones, and W. D. O'Brien, Jr., "Decision directed line detection with application to medical ultrasound," in *Proc. SPIE—Medical Imaging 1996: Image Processing,* vol. 2710, M. H. Loew and K. M. Hanson, Eds., 1996, pp. 698–708.

[35] R. 0. Duda and P. E. Hart, *Pattern Classification and Scene Analysis,* New York: Wiley, 1973.

[36] R. Momenan, R. F. Wagner, B. S. Garra, M. H. Loew, and M. F. Insana, "Image staining and differential diagnosis of ultrasound scans based on the Mahalanobis distance," *IEEE Trans. Med. Imag.,* vol. 13, pp. 37–47, Mar. 1994.

[37] J. D. Foley, A. van Dam, S. K. Feiner, and J. F. Hughes, *Computer Graphics: Principles and Practice,* 2nd ed. Reading, MA: Addison-Wesley, 1987, p. 593.